Multi-phase-field modelling of peritectic, eutectic and monotectic solidification

Britta Nestler
Giesserei Institut, Intzestr. 5, D--52072 Aachen, Germany;
Email: b.nestler@gi.rwth-aachen.de

Adam A. Wheeler
Faculty of Mathematical Studies, Highfield, Southampton SO17 1BJ,
U.K.; Email: aaw@maths.soton.ac.uk

Abstract

A multi-phase-field model for a general class of binary multi-phase alloy systems is proposed to describe the formation of growth structures that are experimentally observed within these systems. The multi-phase-field model is derived in a general form so that it has the flexibility to model and numerically simulate a variety of solidification phenomena in peritectic, eutectic and monotectic alloys by suitably alternating the system parameters. The relation between the free energies in the multi-phase-field model and the specific phase diagram of the alloy system is established by using common tangent constructions. For each type of alloy system, the result of a numerical computation is presented which demonstrates that the new multi-phase-field model exhibits a wide range of realistic complex microstructure evolution. With regards to a peritectic system, the solidification of peritectic solid phase along the properitectic solid phase by solute diffusion in the liquid and the subsequent engulfment of the parent solid phase are investigated in the numerical treatment. The calculation of a eutectic alloy system visualizes the lamellar growth of a eutectic grain into an undercooled melt including the formation of morphological instabilities at the phase boundaries and the nucleation of new lamellae. The final numerical example considers the phase transitions in a monotectic alloy and illustrates typical solidification microstructures in monotectic systems such as coarsening of liquid droplets, particle pushing and the interaction of liquid droplets with a lamellar monotectic front.

First published in:

Introduction

In recent years, the phase-field methodology has been extended to describe polycrystalline grain structures and phase transitions in multi-phase systems. The multi-phase-field model discussed in this paper is based on an ad hoc formulation originally proposed in [1]. This model was further developed to include anisotropy and its sharp interface asymptotic limit was studied in [2] and [3]. Encouraged by these analytical results, numerical simulations of moving grain boundaries and triplejunctions in isotropic as well as in anisotropic polycrystalline systems have been performed in [4] and [5]. In continuation of this work, a crystalline formulation of surface energy anisotropy was suggested in [6] and applied to simulate grain growth in thin metallic films. In this context, the symmetry characteristics of adjacent grain boundary triplejunctions were investigated. Based on the same roots, the multi-phase-field concept was extended to model the solidification in peritectic and eutectic systems, [7] and in monotectic systems including convection within the liquid phases, [8].

The focus of this paper is to construct a thermodynamically consistent formulation of a multi-phase-field model which can be used to model and numerically simulate phase transitions and complex growth structures in peritectic, eutectic and monotectic alloy systems. The model has the generality to describe the solidification processes in all three types of alloys by suitably alternating the system parameters. For each type of alloy, the result of a numerical calculation showing characteristic features of the microstructure evolution is presented.

The Multi-Phase-Field Model

Peritectic, eutectic and monotectic alloy systems consist of three phases. In peritectic and eutectic systems, there is only one liquid phase L, but two solid phases S_1 and S_2. The peritectic reaction $L + S_1 \rightarrow S_2$ occurs when the system is cooled down below the peritectic temperature, whereas the eutectic solidification follows the phase transformation $L \rightarrow S_1 + S_2$ once the temperature of the material sample is below the eutectic point. In a monotectic system, there exist two liquid phases L_1 and L_2 and one solid phase S. Beneath the monotectic temperature, the L_1 phase transforms into L_2 and S according to the reaction $L_1 \rightarrow L_2 + S$.

In order to describe these multiphase systems by a multi-phase-field model, a three-component vector of phase-field variables $\phi(\vec{x}, t) = (\phi_1(\vec{x}, t), \phi_2(\vec{x}, t), \phi_3(\vec{x}, t))$ is introduced. Each phase of the alloy system is associated with one of the components of the vector $\phi(\vec{x}, t)$. Due to the assumption that the alloy system adopts a specific phase state at each point in space, the constraint $\phi_1(\vec{x}, t) + \phi_2(\vec{x}, t) + \phi_3(\vec{x}, t) = 0$ is imposed. The components of the phase-field vector are associated with the phases of the different alloy systems as indicated in Table 1.

Peritectic and eutectic systems		Monotectic systems	
Phase	Phase-field	Phase	Phase-field
S_1 - Solid	$\phi_1(\vec{x}, t)$	L_1 - Liquid	$\phi_1(\vec{x}, t)$
S_2 - Solid	$\phi_2(\vec{x}, t)$	L_2 - Liquid	$\phi_2(\vec{x}, t)$
Liquid L	$\phi_3(\vec{x}, t)$	Solid S	$\phi_3(\vec{x}, t)$

Table 1: The association of the phase-field variables in the multi-phase-field model with the solid and liquid phases of peritectic and eutectic alloys (left) and of monotectic alloys (right).

The multi-phase-field formalism is derived in such a general way that it allows to model all possible phase transitions in peritectic, eutectic and monotectic systems. In addition to the phase-field vector, a concentration variable $c(\vec{x}, t)$ is included into the model formulation. This variable specifies the concentration of a component A of a binary $A - B$ alloy. Furthermore, the system is assumed to be isothermal and the temperature T is treated as a control parameter. The multi-phase-field model is based on a Ginzburg-Landau free energy functional $\mathcal{F}(\phi, c; T)$ which is given by

$$\mathcal{F}(\phi, c; T) = \int_V \mathcal{L}(\phi, \nabla\phi, c; T) \, dV .$$

The Lagrangian energy density $\mathcal{L}(\phi, \nabla\phi, c; T)$ of the system depends on the phase-field vector, on its gradient and on the concentration field. $\mathcal{L}(\phi, \nabla\phi, c; T)$ contains different energy contributions and can be written as

$$\mathcal{L}(\phi, \nabla\phi, c; T) = \sum_{i,k=1, i<k}^{3} \frac{1}{2}\eta_{ik}^2 \, |\phi_i \nabla\phi_k - \phi_k \nabla\phi_i|^2 + f(\phi, c; T),$$

where the constants η_{ik} are gradient energy coefficients which are related to the interface thickness and the surface energy of the interface between the phases labelled i and k. The set of governing evolution equations can be derived from the gradient flow of the energy functional

$$\phi_t = -\frac{1}{\beta(\phi, \nabla\phi)} \frac{\delta \mathcal{F}(\phi, c; T)}{\delta \phi} \tag{1}$$

$$c_t = \nabla \cdot \left\{ M(\phi) \left[c(1-c)\nabla \left(\frac{\delta \mathcal{F}(\phi, c; T)}{\delta c} \right) \right] \right\}, \tag{2}$$

where $\beta(\phi, \nabla\phi)$ characterizes an anisotropic kinetic coefficient and where $M(\phi)$ is defined by

$$M(\phi) = \frac{v_m}{RT} D(\phi), \quad \text{with} \quad D(\phi) = \sum_{i=1}^{3} D_i \phi_i .$$

The constants $D_i, i = 1, \ldots, 3$ are diffusion coefficients of the individual phases. For metallic alloys, the diffusion constants of the solid phases are approximately four orders of magnitude smaller than typical values of the liquid phases. The form of the differential equations ensures that the total free energy decreases monotonically in time and that the total amount of solute concentration in the system is conserved. Next, different expressions for the free energy density $f(\phi, c; T)$ are formulated which allow to characterize the phase transitions in the various types of alloy systems.

For peritectic and eutectic alloy systems, the energy contribution $f(\phi, c; T)$ is specified to be

$$f(\phi, c; T) = \frac{1}{4} \sum_{i,k=1, i<k}^{3} W_{ik}(c)\phi_i^2\phi_k^2 + \sum_i m_i(c; T)\,\phi_i + \frac{RT}{v_m}I(c), \tag{3}$$

where R is the gas constant and v_m ist the molar volume. $I(c)$ represents the entropy of mixing of an ideal solution and is given by

$$I(c) = c\ln(c) + (1-c)\ln(1-c).$$

The coefficients $W_{ik}(c)$ are of the form $W_{ik}(c) = cW_{ik}^B + (1-c)W_{ik}^A$, where the quantities W_{ik}^A and W_{ik}^B are barrier heights between the phases labelled i and k for the case of pure A and pure B, respectively. In a similar way, the functions $m_i(c; T)$ can be expressed as

$m_i(c;T) = c m_i^B(T) + (1-c) m_i^A(T)$. The functions $m_i^A(T)$ and $m_i^B(T)$ are bulk free energies of the pure A and pure B states and can be defined to be

$$m_i^A(T) = L^A \left(\frac{T - T_i^A}{T_i^A} \right) + m_3^A(T) \quad \text{and} \quad m_i^B(T) = L^B \left(\frac{T - T_i^B}{T_i^B} \right) + m_3^B(T),$$

with $i = 1, 2$ and $m_3^B(T) = m_3^A(T) = 0$. The parameters L^A, L^B and $T_i^A, T_i^B, i = 1, 2$ are the latent heat of fusion per unit volume and the melting temperature of the solid phases of the pure component A and B, respectively.

To reflect monotectic solidification processes by the above multi-phase-field model, a different choice for the free energy density $f(\phi, c; T)$ is used which enables to recover a monotectic phase diagram by a common tangent construction in the sharp interface limit. The expression of $f(\phi, c; T)$ for monotectic alloys is

$$f(\phi, c; T) = \frac{1}{4} \sum_{i,k=1, i<k}^{3} W_{ik}(c) \phi_i^2 \phi_k^2 + \sum_{i}^{3} m_i(c; T) \phi_i, \tag{4}$$

with the same definition for the coefficients $W_{ik}(c)$ as in the peritectic and eutectic case. In contrast, the bulk free energies $m_i(c; T)$ of the monotectic phases L_1, L_2 and S are assumed to be

$$m_1(c; T) = \frac{\beta_1}{2} [c - c_1^*(\Delta T)]^2,$$

$$m_2(c; T) = \frac{\beta_2}{2} [c - c_2^*(\Delta T)]^2,$$

$$m_3(c; T) = \frac{\beta_3}{2} [c - c_3^*(\Delta T)]^2 + \Delta T,$$

with $\Delta T = T - T_{mono}$ and $c_i^*(\Delta T) = c_i^0 + \alpha_i \Delta T$. Here, the constants α_i, β_i and c_i^0 determine the form of the phase diagram. An extension of the multi-phase-field model to account for convection in both liquid phases can be found in [8]. In this article, a complete set of dynamic field equations including the fluid flow is derived.

Phase diagrams

The equilibrium solute compositions on either side of a planar stationary interface are related by the common tangent construction to the underlying free energies $f(\phi, c; T)$ of the different bulk phases. Therefore, the phase diagram of a specific alloy can be determined from the parameters in the free energy $f(\phi, c; T)$ by applying the procedure of the common tangent construction. The same energy function $f(\phi, c; T)$ of equation (3) is used to model eutectic and peritectic solidification. To distinguish the two different types of alloys, the parameters $T_1^A, T_2^A, T_1^B, T_2^B$ have to be chosen in a suitable way, see [7] for details. The multi-phase-field model recovers the phase diagram of a eutectic alloy if the parameters in $f(\phi, c; T)$, expression (3) fulfill the relation $\min(T_1^A, T_2^B) > \max(T_2^A, T_1^B)$ or $\min(T_2^A, T_1^B) > \max(T_1^A, T_2^B)$. A peritectic phase diagram is obtained if the parameters in equation (3) satisfy $T_1^A < T_2^A < T_2^B < T_1^B$ or $T_1^A > T_2^A > T_2^B > T_1^B$. In the case of a monotectic system, the free energy $f(\phi, c; T)$ in equation (4) is used to construct a monotectic phase diagram in the sharp interface limit. An example for the set of parameters and for the computation of the common tangent construction for each type of phase diagramm is given in [7] and in [8]. To illustrate these results, Figure 1 shows the Gibbs energies for a peritectic system at three different temperatures and, in the last

image, the computed peritectic phase diagram. A common tangent to all three Gibbs parabolas can be drawn, if the system is at the peritectic temperature, see top right plot of Figure 1.
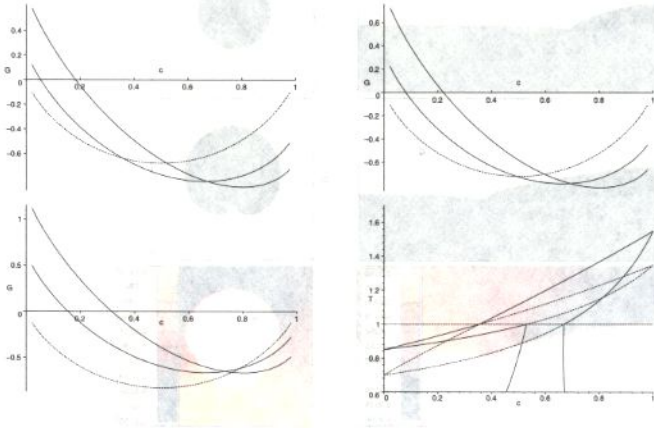

Figure 1: Gibbs energies of the three phases α, β (solid lines) and L (dashed curve) in a peritectic system and at three different temperatures: above the peritectic temperature $T = 1.2$ (top left), at the peritectic temperature $T = 1$ (top right) and below the peritectic temperature $T = 0.98$ (bottom left). The last plot shows the result of a computed peritectic phase diagram including metastable extensions of liquidus and solidus lines by applying a common tangent construction.

Simulations of peritectic, eutectic and monotectic alloys

The objective of this section is to demonstrate the general utility of the multi-phase-field model as a computational vehicle to simulate a wide variety of realistic growth structures and solidification morphologies in peritectic, eutectic and monotectic alloy systems. Pursuing this aim, a selection of numerical solutions of the governing equations (1) and (2) for the phase-field vector $\phi(\vec{x}, t)$ and for the concentration $c(\vec{x}, t)$ is presented. A finite difference discretisation on a uniform rectangular mesh allied to an explicit time marching scheme is used for the three phase-fields and for the solute concentration. For convenience, the phase boundaries are assumed to have isotropic surface energies and effects of fluid flow is ignored. Further details concerning the numerical setup and the system parameters are given in [7] and [8].

First, numerical simulations corresponding to peritectic solidification are reported. The results in Figure 2 a) and b) display the computed dynamical evolution of the three phases in a peritectic system for two different initial configurations. The simulations were carried out at $T = 0.98$ below the peritectic temperature and with zero diffusivities in the two solid phases. The phase diagram shown in Figure 1 (bottom right) was employed. According to the phase diagramm, the equilibrium concentrations of the two solid phases at $T = 0.98$ were set to $c = 0.6670$ and $c = 0.5258$ for the S_1 and S_2 phase, respectively. For the initial concentration in the liquid phase, a mean value of $c = 0.32$ between the S_2 liquidus line and the metastable extension of the S_1 liquidus line was chosen. In both simulations, it can be observed that the peritectic S_2 phase preferentially grows on top of the parent properitectic S_1 phase until the S_2 phase eventually engulfs the S_1 phase. The triplejunctions of all three phases lead the growth direction, because the S_1 phase provides the supply of solute needed for the growth of the S_2 phase and diffusion in the two solid phases is suppressed. The third snapshot in both sequences of Figure 2 a) and b) visualizes the concentration field in the liquid phase during the growth process.
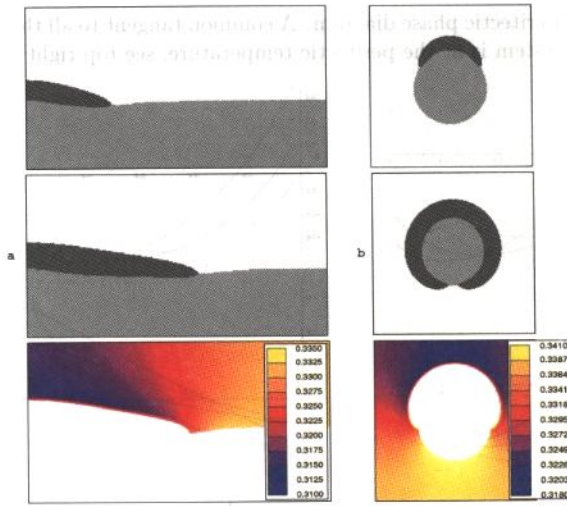
Figure 2: Simulations of peritectic solidification for two different initial phase configurations. The first two snapshots show the distribution of the phases in the computational domain at two different time steps, whereas the last image illustrates the concentration field in the L phase.

The next computation is designed to investigate eutectic phase changes and to demonstrate the extend to which the multi-phase-field model qualitatively reproduces realistic phenomenology of eutectic growth structures. The simulation in Figure 3 refers to the $Al - Si$ alloy system and was performed at $T = 0.9$. The corresponding equilibrium concentrations are $c = 0.0736536303$ for the S_1 phase, $c = 0.84098063$ for the S_2 phase and $c = 0.38$ for the liquid phase L. The snapshots show the concentration field in the liquid during lamellar growth of a eutectic grain into an undercooled melt at different time steps. The simulated structure is compared with an experimental photograph in the last picture of Figure 3. The solid phases S_1 and S_2 are represented as black and white regions. Blue zones of depleted solute ahead of the S_2 lamellae and yellow concentration enriched regions ahead of the S_1 lamellae can be observed. Due to an increase of the lamellar spacing during growth, deep concave hollows are formed at the solid-liquid interfaces and the phase boundaries of the eutectic microstructure evolve in a disordered manner. The subsequent nucleation of solid particles of the opposite phase within the concave portion of the interfaces stabilizes the growth behaviour and re-establishes lamellar growth.

Typical solidification microstructures in monotectic systems are considered in the final calculation, Figure 4. The solid phase S is represented as black and the liquid phase L_2 as white regions. The compositions of the S and L_2 phase were set to its equilibrium values $c = 0.05$ and $c = 0.7$. The L_1 composition was set to an average mean value of $c = 0.375$ between the two liquidus lines of S and L_2. The time sequence in Figure 4 illustrates the coarsening of L_2 droplets in L_1 and their interaction with the L_2/S lamellar front. In a short initial period, L_2 droplets rapidly coarsen with some dissolving completely, others coalescing with larger particles and the remainder growing. In the subsequent longer period, lamellar growth with nucleation of new lamellae, with diffusion controlled pushing of L_2 droplets and with lamellar selection is established.
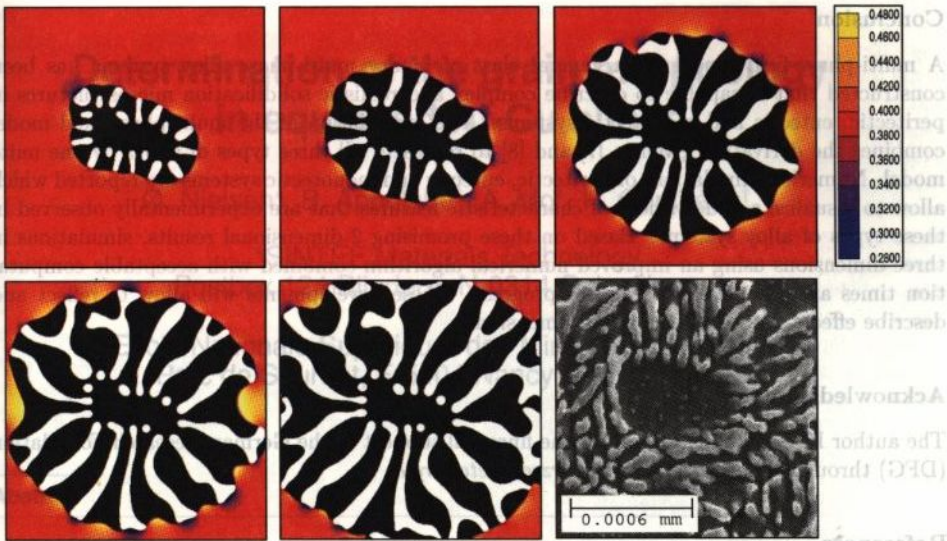
Figure 3: Phase-field simulation of a eutectic $Al - Si$ grain in comparison with an experimental photograph. The snapshots of the calculation display the concentration of silicon and the evolution of the phase boundaries at times $t = 0.00008, 0.00032, 0.00044, 0.00056$ and 0.00068.
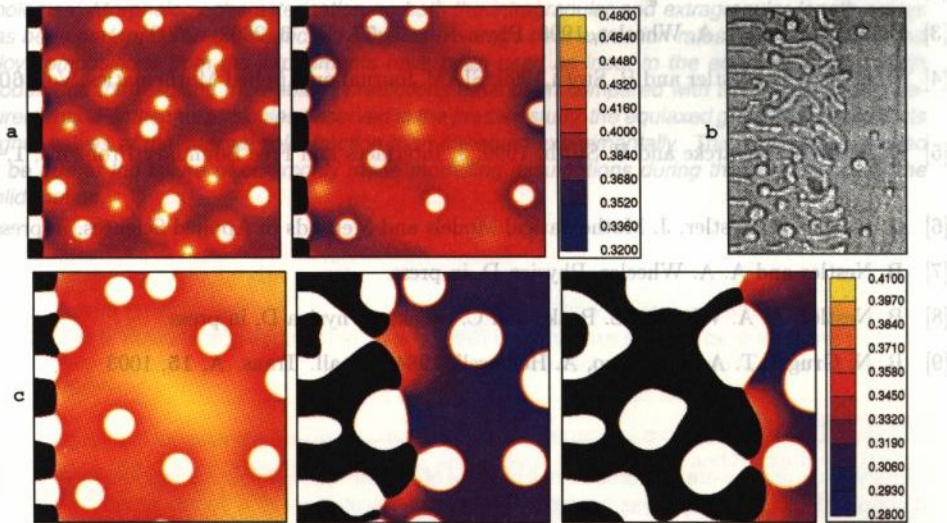

Figure 4: Simulated microstructure formation of a monotectic system with fine dispersed L_2 droplets ahead of a growing lamellar front at times $t = 5.0 \times 10^{-5}, 3.0 \times 10^{-4}$ (first row) and $t = 1.0 \times 10^{-3}, 2.0 \times 10^{-3}, 1.3 \times 10^{-2}$ (second row). The colours visualize the concentration field, where S is represented by black and L_2 by white regions. The first two snapshots correspond to the top right concentration range and show the ripening of L_2 particles of different sizes. The simulation is compared with an experimental monotectic growth pattern b) observed in [9].

Conclusion

A multi-phase-field model for a general class of binary multi-phase alloy systems has been constructed that is capable to describe complex and realistic solidification microstructures in peritectic, eutectic and monotectic systems. The formulation of the multi-phase-field model combines the derivation given in [7] and [8] to represent all three types of alloys by one unite model. Numerical simulations of peritectic, eutectic and monotectic systems are reported which allow to visualize a wide variety of characteristic features that are experimentally observed in these types of alloy systems. Based on these promising 2-dimensional results, simulations in three dimensions using an improved numerical algorithm combined with acceptable computation times are planned in our future progress. These developments will allow to reflect and describe effects due to three spatial dimensions.

Acknowledgements

References

[1] I. Steinbach, F. Pezzolla, B. Nestler, M. Seesselberg, R. Prieler, G. J. Schmitz and J. L. L. Rezende, 1996, Physica D, **94**, 135–147

[2] H. Garcke, B. Nestler and B. Stoth, 1998, Physica D **115**, 87 - 108

[3] B. Nestler and A. A. Wheeler, 1998, Phys. Rev. E **57**, No. 3, 2602 - 2609

[4] H. Garcke, B. Nestler and B. Stoth,1999, SIAM Journal on Applied Mathematics, Vol. **60**, No. 1, 295-315

[5] B. Nestler, H. Garcke and B. Stoth, 1999, J. Interfaces and Free Boundary Problems, **1**, 175 - 198

[6] H. Garcke, B. Nestler, J. Mathematical Models and Methods in Applied Sciences, in press

[7] B. Nestler and A. A. Wheeler, Physica D, in press

[8] B. Nestler, A. A. Wheeler, L. Ratke and C. Stöcker, Physica D, in press

[9] R. N. Grugel, T. A. Longrasso, A. Hellawell, 1984, Metall. Trans. A, **15**, 1003